J. Fluid Mech. (1991), *vol.* 226, *pp.* 549–564
Printed in Great Britain

Twist vortices and their instabilities in the Taylor–Couette system

By E. WEISSHAAR, F. H. BUSSE AND M. NAGATA†
Institute of Physics, University of Bayreuth, 858 Bayreuth, Germany

(Received 8 December 1989 and in revised form 23 November 1990)

The problem of three-dimensional flows arising from the twist instability of Taylor vortices is investigated numerically in the narrow gap limit of the Taylor–Couette system with nearly corotating cylinders. There are two types of twist vortices: those that do not deform the in- and outflow boundaries of the Taylor vortices and those that do. The latter type are called wavy twist vortices and correspond to class II of Nagata (1986). The stability of the twist vortices with respect to arbitrary infinitesimal disturbances is analysed with the result that the twist solutions are unstable within a large part of the parameter space with respect to Eckhaus and skewed-varicose-type instabilities. An analytical model is described which fits the numerical results on the transition from axisymmetric vortices to unstable twist solutions. The theoretical findings are compared with experimental observations.

1. Introduction

Apart from Rayleigh–Bénard convection, Taylor–Couette flow between differentially rotating cylinders is the best known system for the study of subsequent transitions leading from simple to more complex forms of fluid motion. Because of the particular direction of the axis of rotation and because of the different radii of the cylinders the Taylor–Couette system exhibits fewer symmetries than a horizontally extended Rayleigh–Bénard layer with a Boussinesq fluid. In the limit of a small gap between the two coaxial cylinders an additional symmetry is gained, however, and the Taylor–Couette system becomes equivalent with respect to its symmetries to a Rayleigh–Bénard layer of an electrically conducting fluid with an imposed horizontal magnetic field, for instance. In fact, the two-dimensional rolls, which are the preferred mode at the onset of instability, and the Taylor vortices represent mathematically identical solutions of the basic equations if the temperature of the Rayleigh–Bénard layer is identified with the azimuthal velocity field of the Taylor–Couette system and if the Prandtl number is set equal to unity.

Systems with high degrees of symmetry are especially useful for theoretical investigations of transitions to complex forms of fluid flow. While the basic solution reflects the symmetry of the external conditions, one or more symmetries are usually broken as bifurcations occur. Axisymmetric Taylor vortices are introduced over a wide range of the parameter space as the first instability as the Reynolds number is increased. The axisymmetry is usually broken through the secondary instability and a variety of three-dimensional flows is introduced depending on the position in the parameter space. Wavy vortices and twist vortices appear to be the most widely observed flows in small-gap experiments (Andereck, Dickman & Swinney 1983).

† Present address: Department of Mathematics, The University of Birmingham, Birmingham B15 2TT, UK.

Much of the theoretical effort has thus been focused on these types of flow. Computations of three-dimensional wavy vortex flow have been presented by Marcus (1984) and Moser, Moin & Leonhard (1983) in the case of a finite gap. In the present paper we shall adopt the limit of a small gap in the case of nearly corotating cylinders since it allows the following theoretical simplifications:

(i) The axisymmetric solution depends on only a single external parameter in this limit. In fact, it becomes mathematically identical to convection rolls in a fluid of Prandtl number unity.

(ii) The additional symmetry of this limit permits the separation of the infinitesimal three-dimensional disturbances into two classes. Moreover, because the averaged flow vanishes in the particular frame of reference rotating with the mean angular velocity of the two cylinders, most of the growing disturbances correspond to monotonic bifurcations.

(iii) The latter property permits the description of several non-axisymmetric vortex flows in the form of stationary solutions of the basic equations with respect to the particular frame of reference.

(iv) The stability of the stationary tertiary flow states can be investigated relatively easily by an extension of the analysis used to study the stability of axisymmetric Taylor vortices.

The stationarity of certain tertiary flow states can also be achieved, of course, in the case of a finite gap by a suitable adjustment of the rotation rate of the reference frame. This rotation rate does not correspond to the mean angular velocities of the cylinders, however, and thus cannot be predicted *a priori*. Instead it varies with the amplitude of the tertiary flow.

The simplifications (i)–(iii) have been already used by Nagata (1986, 1988) who studied the stability of Taylor vortices over a wide range of the parameter space within the small-gap approximation and also obtained three-dimensional solutions describing wavy vortices. In the present paper finite-amplitude twist and wavy twist solutions will be studied numerically by the same methods as used in Nagata (1986, 1988) and in the earlier work by Nagata & Busse (1983). For the first time a stability analysis of tertiary flow states will be included in the analysis, which permits the identification of the third subsequent bifurcation of the system. Some preliminary results of the present analysis have been reported at a recent conference (Weisshaar, Busse & Nagata 1990).

A wealth of information on three-dimensional flows in the Taylor–Couette system has become available in recent years through the work of Andereck *et al.* (1983) and Andereck, Lin & Swinney (1986). Although the ratio of inner to outer radius of the independently rotating cylinders was only about 0.88, the agreement between theoretical predictions and experimental observations for the onset of Taylor vortices and secondary instabilities is remarkably good. We shall return to questions of comparisons in §§3 and 4.

The paper starts with an outline of the mathematical technique in §2. The Galerkin method will be employed and steady finite-amplitude solutions are obtained by the Newton–Raphson iteration method. The three-dimensional twist vortex solutions are described in §3 and their stability is analysed in §4. Concluding remarks are offered in §5.

2. Mathematical formulation of the problem

We consider the flow in the narrow gap between two coaxial cylinders with radii R_1 and R_2 and rotating with speeds $\Omega_1 R_1$ and $\Omega_2 R_2$, respectively. The gap width $d \equiv R_2 - R_1$ will be used as lengthscale in the following and d^2/ν as timescale, where ν is the kinematic viscosity of the fluid. We introduce a Cartesian system of coordinates with the x-coordinate in the radial direction, the y-coordinate in the azimuthal direction and the z-coordinate in the direction of the axis as shown in figure 1. The corresponding unit vectors will be denoted by $\boldsymbol{i}, \boldsymbol{j}, \boldsymbol{k}$. The dimensionless Navier–Stokes equations can then be obtained in the form

$$\left(\frac{\partial}{\partial t} + \boldsymbol{u}\cdot\boldsymbol{\nabla}\right)\boldsymbol{u} + \Omega \boldsymbol{k}\times\boldsymbol{u} = -\boldsymbol{\nabla}\pi + \nabla^2\boldsymbol{u}, \tag{2.1a}$$

$$\boldsymbol{\nabla}\cdot\boldsymbol{u} = 0, \tag{2.1b}$$

where Ω is twice the mean rotation rate in dimensionless units,

$$\Omega = (\Omega_1 + \Omega_2)\, d^2/\nu. \tag{2.2}$$

The boundary conditions are given by

$$\boldsymbol{u} = \mp \tfrac{1}{2}\mathscr{R}\boldsymbol{j} \quad \text{at} \quad x = \pm\tfrac{1}{2}, \tag{2.3}$$

where the Reynolds number $\mathscr{R}$ is defined by

$$\mathscr{R} \equiv (\Omega_1 - \Omega_2)(R_1 + R_2)\, d/2\nu. \tag{2.4}$$

It is convenient to eliminate the equation of continuity (2.1b) by the introduction of the following general representation of the velocity field:

$$\boldsymbol{u} = (-\mathscr{R}x + V(x))\boldsymbol{j} + \boldsymbol{\nabla}\times(\boldsymbol{\nabla}\times\boldsymbol{i}\phi) + \boldsymbol{\nabla}\times\boldsymbol{i}\psi. \tag{2.5}$$

By using the operations $\boldsymbol{i}\cdot\boldsymbol{\nabla}\times(\boldsymbol{\nabla}\times\ldots,)$ and $\boldsymbol{i}\cdot\boldsymbol{\nabla}\times$ on equation (2.1a) we obtain two equations for ϕ and ψ:

$$\left(\nabla^2 - \frac{\partial}{\partial t}\right)\nabla^2\Delta_2\phi - \Omega\frac{\partial}{\partial z}\Delta_2\psi = (-\mathscr{R}x + V)\frac{\partial}{\partial y}\nabla^2\Delta_2\phi - \frac{\partial^2}{\partial x^2}V\frac{\partial}{\partial y}\Delta_2\phi + \boldsymbol{i}\cdot\boldsymbol{\nabla}\times(\boldsymbol{\nabla}\times(\boldsymbol{u}\cdot\boldsymbol{\nabla}\boldsymbol{u})), \tag{2.6a}$$

$$\left(\nabla^2 - \frac{\partial}{\partial t}\right)\Delta_2\psi + \Omega\frac{\partial}{\partial z}\Delta_2\phi = (-\mathscr{R}x + V)\frac{\partial}{\partial y}\Delta_2\psi + \left(\mathscr{R} - \frac{\partial}{\partial x}V\right)\frac{\partial}{\partial z}\Delta_2\phi - \boldsymbol{i}\cdot\boldsymbol{\nabla}\times(\boldsymbol{u}\cdot\boldsymbol{\nabla}\boldsymbol{u}), \tag{2.6b}$$

$$\left(\frac{\partial^2}{\partial x^2} - \frac{\partial}{\partial t}\right)V = -\frac{\partial}{\partial x}\overline{\Delta_2\phi\left(\frac{\partial^2}{\partial x\,\partial y}\phi + \frac{\partial}{\partial z}\psi\right)}. \tag{2.6c}$$

The third equation (2.6c) for the azimuthal mean flow $V(x)$ is obtained when the y-component of (2.1a) is averaged over cylinders $x = \text{const}$. This average is indicated by a bar. The operator Δ_2 is defined by $\Delta_2 \equiv \nabla^2 - (\boldsymbol{i}\cdot\boldsymbol{\nabla})^2$.

The boundary condition (2.3) implies the conditions

$$\phi = \frac{\partial}{\partial x}\phi = \psi = V = 0 \quad \text{at} \quad x = \pm\tfrac{1}{2}. \tag{2.7}$$

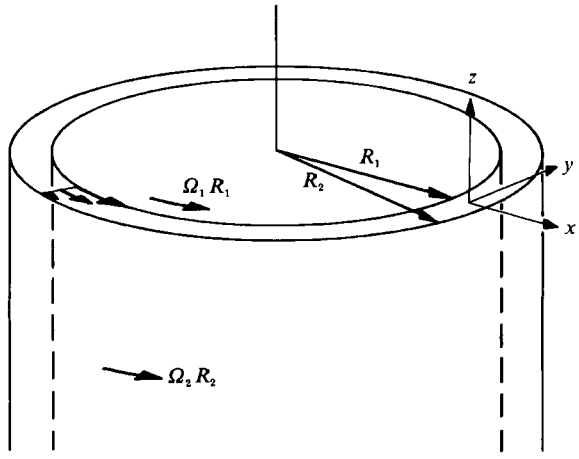

FIGURE 1. The Taylor–Couette system.

The small-gap approximation for nearly corotating cylinders is defined by

$$\frac{|\Omega_2-\Omega_1|}{|\Omega_2+\Omega_1|} \ll 1, \quad \frac{R_2-R_1}{R_2+R_1} \ll 1, \tag{2.8}$$

where the ratio of the two quantities on the left-hand sides will be finite in general. While the trivial solution $\phi \equiv \psi \equiv V \equiv 0$ exists everywhere, it is unstable with respect to y-independent disturbances in the form of Taylor vortices when the condition

$$(\mathscr{R}-\Omega)\,\Omega \geqslant 1708 \tag{2.9}$$

is satisfied. The Taylor vortices are mathematically identical to convection rolls in a fluid layer of Prandtl number unity heated from below. But this analogy ends when three-dimensional effects are considered and the parameters $\mathscr{R}, \Omega$ no longer appear in the problem only in the combination $(\mathscr{R}-\Omega)\,\Omega$. In Nagata (1986) the stability of the y-independent Taylor vortex solutions was investigated with respect to arbitrary disturbances. Here we are interested in the three-dimensional solutions generated by growing twist-type disturbances.

The instabilities of class 1 and class 2 studied in Nagata (1986) correspond to a wavy modulation of the Taylor vortices in the azimuthal direction and exhibit either the same symmetry in the z-direction as in the vortex solution or the symmetry of a small translation of that solution. We shall refer to the former case as the twist instability, and the latter as the wavy twist instability. At finite amplitudes of the disturbances the three-dimensional solutions can be described by

$$\phi = \sum_{m,n,l} a_{mnl} \begin{Bmatrix} \cos m\alpha y \\ \sin m\alpha y \end{Bmatrix} \cos n\gamma z f_l(x), \tag{2.10a}$$

$$\psi = \sum_{m,n,l} b_{mnl} \begin{Bmatrix} \cos m\alpha y \\ \sin m\alpha y \end{Bmatrix} \sin n\gamma z \sin l\pi(x-\tfrac{1}{2}), \tag{2.10b}$$

and by

$$\phi = \sum_{m,n,l} (\hat{a}_{mnl} \cos n\gamma z + a_{mnl} \sin n\gamma z) \begin{Bmatrix} \cos m\alpha y \\ \sin m\alpha y \end{Bmatrix} f_l(x), \tag{2.11a}$$

$$\psi = \sum_{m,n,l} (\hat{b}_{mnl} \sin n\gamma z + b_{mnl} \cos n\gamma z) \begin{Bmatrix} \cos m\alpha y \\ \sin m\alpha y \end{Bmatrix} \sin l\pi(x-\tfrac{1}{2}), \tag{2.11b}$$

where the upper functions in the wavy bracket correspond to even $n+l$ while the lower functions must be chosen for odd $n+l$. In the case of (2.11) the coefficients $\hat{a}_{mnl}, \hat{b}_{mnl}$ vanish for odd m and the coefficients a_{mnl}, b_{mnl} vanish for even m. The expansion functions $f_l(x)$ vanish with their derivatives at $x = \pm\frac{1}{2}$. For their definition we refer to Nagata (1986) or to Chandrasekhar (1961, p. 635). In both (2.10) and (2.11) the modification of the mean zonal flow is given by

$$V = \sum_k c_k \sin 2k\pi x \tag{2.12}$$

since the mean flow must be antisymmetric with respect to the midplane of the fluid layer for reasons of symmetry.

Both (2.10) and (2.11) describe the Taylor vortex flow in the case when coefficients with $m > 0$ vanish. Solution (2.10) is called twist solution since the terms with $m > 0$ do not distort the boundary between neighbouring vortices. We choose the name wavy twist for (2.11) because then periodic shift of the boundary between neighbouring vortices gives the twisted vortices a wavy appearance. It belongs to the same symmetry class as the wavy Taylor vortex according to the Iooss (1986) classification scheme. While wavy Taylor vortices are characterized by a finite phase speed relative to the frame of reference rotating with the mean rotation rate, both twist solutions are stationary with respect to this frame in the small-gap limit.

The stability of steady solutions of the form (2.10) or (2.11) can be investigated by superimposing infinitesimal disturbances,

$$\tilde{\phi} = \sum_{m,n,l} \tilde{a}_{mnl} \exp\{\mathrm{i}(n\gamma+b)z + \mathrm{i}(m\alpha+d)y + \sigma t\} f_l(x), \tag{2.13a}$$

$$\tilde{\psi} = \sum_{m,n,l} \tilde{b}_{mnl} \exp\{\mathrm{i}(n\gamma+b)z + \mathrm{i}(m\alpha+d)y + \sigma t\} \sin l\pi(x-\tfrac{1}{2}), \tag{2.13b}$$

$$\tilde{V} = \sum_k \tilde{c}_k \sin 2\pi k x. \tag{2.13c}$$

The equations for the coefficients $\tilde{a}_{mnl}, \tilde{b}_{mnl}, \tilde{c}_k$ are linear homogenous with the complex growth rate σ as eigenvalue. Unless b and d both vanish, $\tilde{V}$ must be neglected. For a given steady solution characterized by the parameters $\alpha, \gamma, \mathscr{R}$, and Ω the eigenvalues σ can be determined as a function of the wavenumber parameters b and d. Whenever an eigenvalue σ with positive real part σ_r is found, the steady solution is unstable. Otherwise we shall regard it as stable. In the following we shall first discuss the properties of the steady solutions (2.10) and (2.11) and then analyse their stability.

3. Steady twist solutions

3.1. *Onset of twists*

The twist instability breaks the symmetry with respect to the axis of rotation, and introduces an azimuthal variation with the basic wavenumber α. When the Reynolds number is increased there exists a critical value of α at which the twist instability first occurs. This preferred value of α will be assumed in the following unless we indicate otherwise. Hence a twist solution is characterized by its symmetry class and the set of parameters $\mathscr{R}$, $\Omega\mathscr{R}$, and γ. Figure 2 (*a*) shows curves of the critical Reynolds numbers $\mathscr{R}_{\mathrm{II}}$ for the onset of the twist instability as a function of $\Omega/\mathscr{R}$ for several values of the axial wavenumber γ. It is evident that the critical Reynolds number decreases monotonically with increasing axial wavelength of the vortices, while for

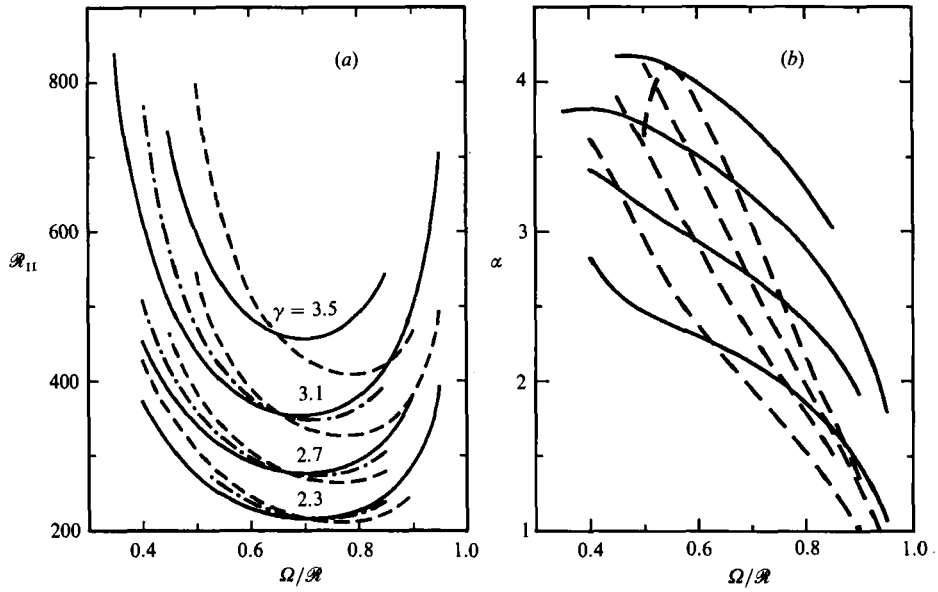

FIGURE 2. (*a*) The onset of twist modes as a function of the rotation rate $\Omega/\mathscr{R}$ for various wavenumbers γ. The solid line corresponds to ordinary twists and the dashed line to wavy twists, and the dash-dotted lines correspond to the onset of subharmonic disturbances. (*b*) The wavenumber α in the azimuthal direction for the growing disturbances of (*a*).

fixed γ the smallest critical Reynolds number is achieved at rotation rates in the interval $0.6 < \Omega/\mathscr{R} < 0.8$. In this region the neutral curve for the onset of wavy twists also intersects the neutral curve of ordinary twists. Ordinary twists are preferred at low rotation rates, while wavy twists are preferred at high rotation rates. In figure 2(*a*) we have also plotted the Reynolds number for the onset of a subharmonic instability corresponding to $b = \frac{1}{2}\gamma$ in (2.12). This instability can be regarded as a combination of the two twist instabilities which are coupled by the Floquet factor $\exp\{ibz\}$. It is thus not surprising that its onset occurs at an intermediate Reynolds number. It does not seem to become the preferred instability anywhere and its physical significance is thus doubtful.

A direct comparison with experimental results obtained by Andereck *et al.* (1983) can be done after the parameters $\mathscr{R}$ and Ω have been transformed into the parameters $\mathscr{R}_1$ and $\mathscr{R}_0$, which are the inner and the outer Reynolds number used in the cited experiments. The transformation relation (see also Nagata 1986) is given by

$$\mathscr{R}_1 = \tfrac{1}{2}q\left(\frac{\Omega}{1-q}+\frac{2\mathscr{R}}{1+q}\right), \quad \mathscr{R}_0 = \frac{1}{2}\left(\frac{\Omega}{1-q}+\frac{2\mathscr{R}}{1+q}\right), \tag{3.1a, b}$$

where $q = 0.883$ is the cylinder radius ratio used in the experiments. In figure 3(*a*, *b*) critical curves for the onset of twists for two fixed outer Reynolds numbers, namely $\mathscr{R}_0 = 815$ and 1060, are compared with experiments. At $\mathscr{R}_0 = 815$ (figure 3*a*) the experimental data cover rotation rates in the range $0.58 < \Omega/\mathscr{R} < 0.83$ while at $\mathscr{R}_0 = 1060$ (figure 3*b*) they cover the interval $0.78 < \Omega/\mathscr{R} < 0.90$. Only ordinary twists seem to have been observed in the experiments. The observed wavelength in the azimuthal direction nearly matches the wavelength of the Taylor vortices in the axial direction, which agrees well in the relevant regime with the theoretical findings shown in figure 2(*b*). The observed onset is shifted with respect to the solid lines in

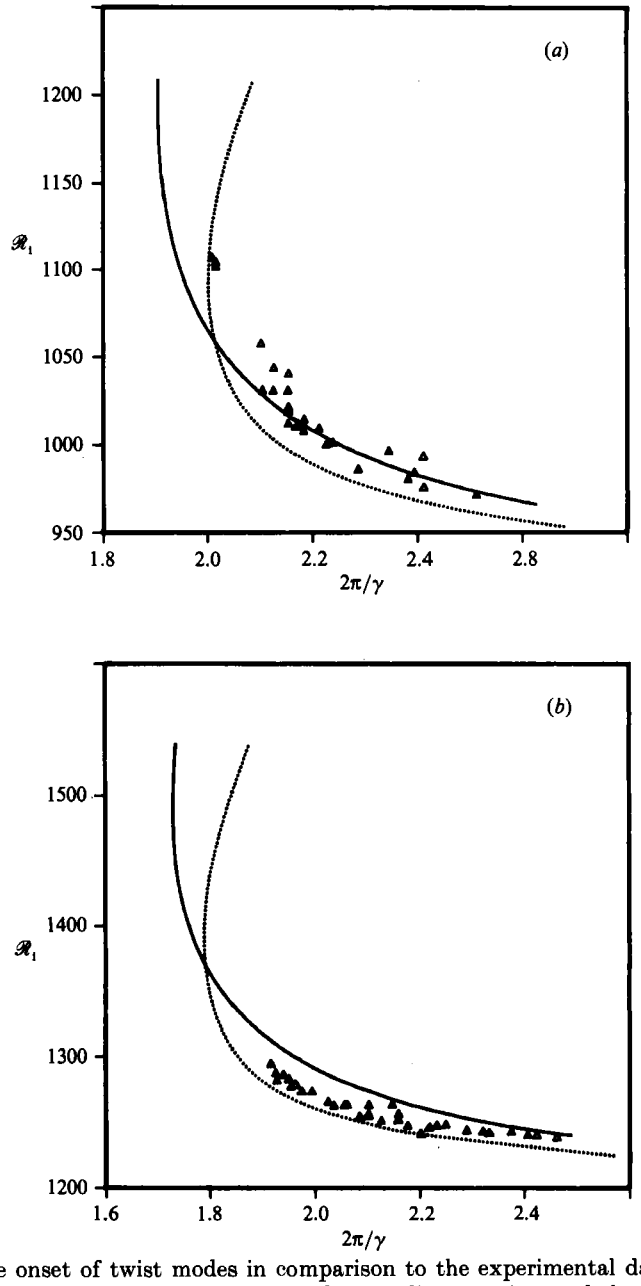

FIGURE 3. The onset of twist modes in comparison to the experimental data by Andereck *et al.* (1983) (symbols). The solid curve corresponds to ordinary twists and the dotted curve to wavy twists. The outer Reynolds number is (*a*) $\mathscr{R}_0 = 815$, (*b*) $\mathscr{R}_0 = 1060$.

figure 3 (*a*, *b*). But this shift can be attributed to the effect of a finite gap width in the experiment. While the critical Reynolds number for the onset of ordinary twists seems to be somewhat lowered by the finite-gap effect, at least for lower values of γ, the opposite shift seems to occur for the onset of wavy twists, since there appears to be no experimental evidence for them.

		Torque τ				
	$\mathscr{R}$	2D	3D ($N_T = 10$)	3D ($N_T = 9$)	$\Omega/\mathscr{R}$	α
Ordinary twists $\mathscr{R}_{II} = 397.67$	412.1	964.79	958.68	958.15	0.55	3.62
	401.1	928.34	926.93	926.36		
Wavy twists $\mathscr{R}_{II} = 327.53$	348.1	501.28	498.75	498.70	0.80	1.98
	332.4	473.31	472.85	472.76		

TABLE 1. Torque τ of a Taylor vortex and for twist solutions with $\gamma = 3.1$

3.2. *Finite-amplitude solutions*

For the calculation of finite-amplitude solutions a proper choice of truncation parameters is necessary. This choice is problem-dependent and is also influenced by the computer storage requirements of the stability analysis. Several truncation formulae were tested. The following formula for the subscripts of the coefficients that are taken into account in (2.10), (2.11) turned out to optimize computer storage:

$$l + |m| + |n| \leqslant N_T. \tag{3.2a}$$

In addition we introduce an extra truncation for m:

$$|m| \leqslant m_T. \tag{3.2b}$$

Since the same truncation formulae must be applied for the stability analysis of twist vortex flow for reasons of consistency, the values 10 and 4 were usually chosen for N_T and m_T, respectively, in order to satisfy the storage requirements. This truncation procedure was also used in the case of the axisymmetric Taylor vortices discussed in §3.1.

The finite-amplitude solutions have the following general properties. All twist solutions bifurcate supercritically when the azimuthal wavenumber α at which the instability sets in first is used. No subcritical solutions were found. Solutions with different values of α exist at Reynolds numbers above $\mathscr{R}_{II}$. At higher Reynolds numbers there is some ambiguity in the choice of α. We assume constant α on lines $\Omega/\mathscr{R} = \text{const.}$ and $\gamma = \text{const.}$ in the parameter space. Coefficients with subscripts $m = 1$ increase proportional to $\epsilon^{\frac{1}{2}}$, where $\epsilon = \mathscr{R} - \mathscr{R}_{II}$ is a small deviation from the threshold Reynolds number $\mathscr{R}_{II}$ for twists. Solutions have been computed for a finite range of ϵ above threshold.

A useful characterization of finite-amplitude solutions is given by the torque $\tau = \mathrm{d}V/\mathrm{d}x|_{x=\mp\frac{1}{2}}$, which is exerted on the cylinders. In table 1 the torques of two representative twist solutions of each symmetry class are compared with values of τ of the (unstable) two-dimensional solutions at the same points in the parameter space. The torques of the tertiary flows increase with Reynolds number but are always smaller than the corresponding torque of the axisymmetric Taylor vortex flow. Hence the twist instability reduces the increase of the torque with Reynolds number. The torque τ can also be used as a sensitive measure of convergence. In table 1 the torques of tertiary flows obtained for the truncation condition $N_T = 9$ are also displayed. The values obtained by the two truncation conditions differ by only 0.02%. Individual coefficients may show somewhat larger changes since the addition of high-order coefficients at higher truncation is compensated by a readjustment of low-order coefficients. This effect may be seen in table 2 where mean flow coefficients

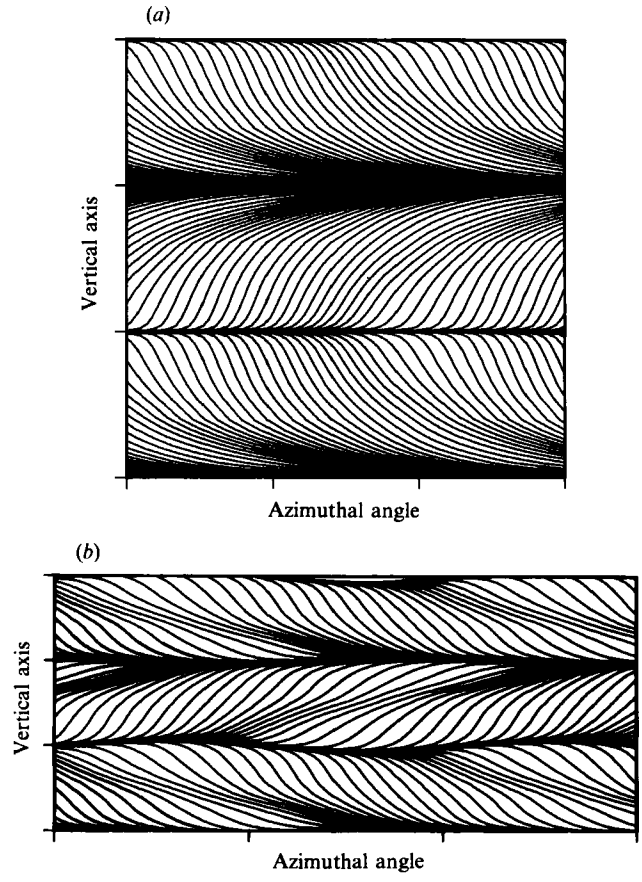

FIGURE 4. (*a*) Ordinary twist solution at $\mathscr{R} = 271.6$, $\gamma = 2.3$, $\alpha = 2.63$, $\Omega/\mathscr{R} = 0.55$. The streamlines near the outer wall are plotted. (*b*) Wavy twist solution at $\mathscr{R} = 640$, $\gamma = 2.8$, $\alpha = 1.23$, $\Omega/\mathscr{R} = 0.9$. The streamlines of shear near the outer wall are plotted.

k	$N_T = 9$	$N_T = 10$
1	12.28870987	12.28486500
2	−1.41308995	−1.41606455
3	−0.00984295	−0.00957502
4	0.10242039	0.08318781
5	−0.02726337	−0.04443247
6	0.01075080	0.00873440
7	−0.00474061	−0.00424608
8	0.00231991	0.00218639
9		0.00119623

TABLE 2. Mean flow coefficients c_k for $\mathscr{R} = 267.49485$, $\Omega = 0.8\mathscr{R}$, $\gamma = 2.7$, $\alpha = 1.791$

have been listed for different truncation levels. The total influence of the shear is changed little as the addition of the 9th coefficients is compensated by a corresponding decrease of lower-order coefficients.

Figures 4(*a*) and 4(*b*) give an impression of the image of the twist vortices as they would appear to the observer. We have drawn streamlines based on $\mathrm{d}\boldsymbol{u}/\mathrm{d}x|_{x=\frac{1}{2}}$ instead of on the velocity field $\boldsymbol{u}$ since the latter vanishes at $x = \frac{1}{2}$. The particles used for flow

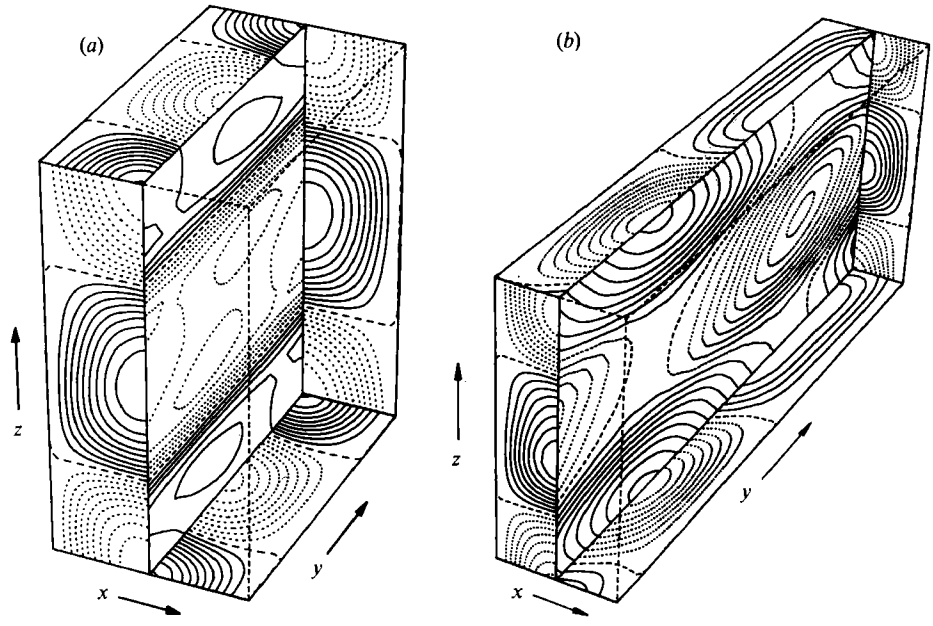

FIGURE 5. (a) Ordinary twist solution at $\mathscr{R} = 271.6$, $\gamma = 2.3$, $\alpha = 2.63$, $\Omega/\mathscr{R} = 0.55$. (b) Wavy twist solution at $\mathscr{R} = 640$, $\gamma = 2.8$, $\alpha = 1.23$, $\Omega/\mathscr{R} = 0.9$. The plots show a three-dimensional representation of the flow by isolines of the potentials ψ, $\partial\phi/\partial z$ and $-\partial\phi/\partial y$ in the planes perpendicular to the unit vectors $\boldsymbol{i}, \boldsymbol{j}$ and $\boldsymbol{k}$, respectively.

visualization usually align themselves with the shear and should produce a similar image. The streamlines of the shear clearly reproduce the typical twist structure. The plots are presented with the correct aspect ratio of axial and azimuthal wavelength. For ordinary twists (figure 4*a*) this aspect ratio agrees well with that seen in the photographs published by Andereck *et al.* (1983, 1986). The axial wavelength is larger by a factor of 1.3 than the azimuthal wavelength. By contrast, the azimuthal wavelength of wavy twists is significantly longer than the axial wavelength in the parameter regime where they are preferred. Unfortunately photographs of structures which may be related to wavy twists are not available.

The fluctuating velocity field can be written in the form $\boldsymbol{u} = \boldsymbol{\nabla}\times\boldsymbol{i}\psi + \boldsymbol{\nabla}\times\boldsymbol{j}\phi_1 + \boldsymbol{\nabla}\times\boldsymbol{k}\phi_2$, where $\boldsymbol{i}, \boldsymbol{j}$ and $\boldsymbol{k}$ are the unit vectors in the x-, y- and z-directions, respectively, and $\phi_1 = \partial\phi/\partial z$, $\phi_2 = -\partial\phi/\partial y$ are derivatives of the potential ϕ. This formula allows a three-dimensional graphic representation of the velocity field through contour plots of ψ, ϕ_1 and ϕ_2 in the planes perpendicular to $\boldsymbol{i}, \boldsymbol{j}, \boldsymbol{k}$ as shown for typical examples in figure 5(*a*, *b*).

4. Stability of twisted vortices

With the truncation parameters $N_T = 10$ and $m_T = 4$ the matrix for the coefficients $\tilde{a}_{l,m,n}$, $\tilde{b}_{l,m,n}$ and $\tilde{c}_k$ attains a rank of 758. However, when one of the Floquet parameters d or b vanishes the eigenvectors separate into two independent subclasses and the size of the matrix is halved. Fortunately, typical properties of the instabilities can be studied in cases when either b or d vanishes. In many cases, however, the full problem has also been solved.

The results of the stability analysis are summarized in figure 6, where the neutral curves for the onset of twists are displayed in the three-dimensional parameter space

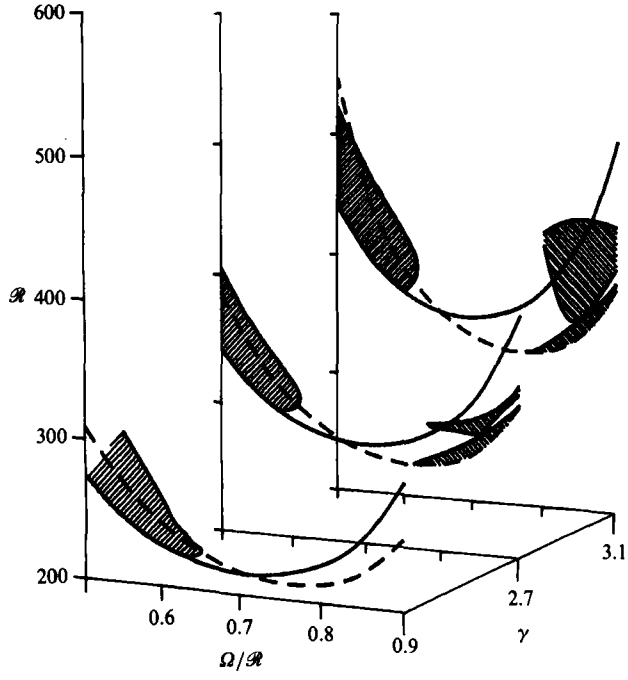

FIGURE 6. The results of the stability analysis in the cases $\gamma = 2.3, 2.7, 3.1$ have been combined in order to give an impression of the three-dimensional nature of the stability regions. The solid lines represent the onset of twist solutions, while the hatched areas indicate the stable regimes of twist solutions.

$(\Omega/\mathscr{R}, \gamma, \mathscr{R})$. We have included three curves, for the axial wavenumbers $\gamma = 2.3$, 2.7 and 3.1. The hatched areas denote regimes of stable twist vortices. In the following we shall describe the various instabilities of twisted vortices on the basis of this diagram. Only twist solutions with Reynolds numbers $\mathscr{R}$ in the interval $0 \leqslant \mathscr{R} - \mathscr{R}_{\mathrm{II}} \leqslant 60$ have been analysed with respect to their stability. Regimes of stable solutions that may eventually exist above these Reynolds numbers have not been considered in the plot.

While ordinary twists are preferred at low rotation rates and wavy twists at high rotation rates, the regions of existence of the two twist solutions overlap to a considerable extent. The twist solution that is not preferred because of a higher critical Reynolds number will usually be unstable with respect to disturbances with the tendency to realize the other twist solution. But at intermediate rotation rates both twist solutions are found to be unstable, as shown in figure 6. The mechanism of instability resembles an Eckhaus-type instability in that the growth rate σ is real and tends to grow proportionally to b^2. This instability sets in at the threshold of twist solutions for arbitrary small b. In the limit $b \to 0$ the disturbance corresponds to a translation or shift of the twist solution in the z-direction with a positive second derivative $\sigma_{\mathrm{s}}'' \equiv \mathrm{d}^2\sigma_{\mathrm{s}}/\mathrm{d}b^2|_{b=0}$. The b-value of the maximum growth rate increases with increasing distance from the threshold. Below threshold, however, the axisymmetric Taylor–Couette vortices are stable and σ_{s}'' jumps from negative to positive values across the threshold. This discontinuity originates from the degeneracy of the eigenvector space spanned by the shifting mode and by the twist mode. Below threshold the growth rates for small b are given by

$$\sigma_{\mathrm{s}} = -a_1 b^2, \quad \sigma_{\mathrm{t}} = -a_2 b^2 + c_1(\mathscr{R} - \mathscr{R}_{\mathrm{II}}). \tag{4.1}$$

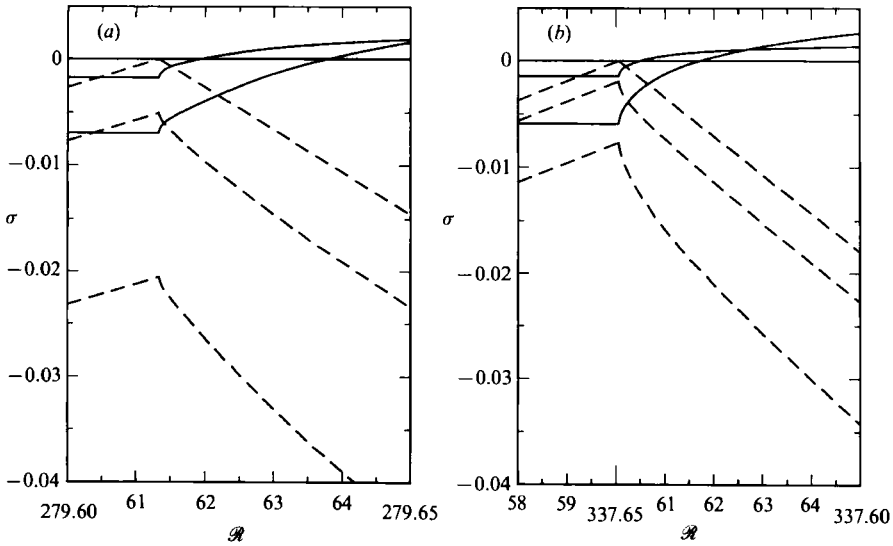

FIGURE 7. Growth rates for the shifting (solid lines) and twist (dashed lines) modes as function of the Reynolds number for (*a*) ordinary twists with $\alpha = 2.8163$, $\gamma = 2.7$, and (*b*) wavy twists with $\alpha = 2.66$, $\gamma = 3.1$. The b-values are 0, 0.025, 0.05 for the upper, middle and lower curves on the left-hand sides.

The eigenvector of the shifting mode exhibits components with $m = 0$ only, while the twist mode has non-axisymmetric components with $m = 1$. Above threshold they are coupled by the action of the non-axisymmetric components of the finite-amplitude solutions

$$\begin{vmatrix} \sigma + a_1 b^2 & (\mathscr{R} - \mathscr{R}_{\mathrm{II}})^{\frac{1}{2}} b c_3 / c_4 \\ (\mathscr{R} - \mathscr{R}_{\mathrm{II}})^{\frac{1}{2}} b c_4 & \sigma + a_2 b^2 + c_2(\mathscr{R} - \mathscr{R}_{\mathrm{II}}) \end{vmatrix} = 0. \tag{4.2}$$

The two growth rates are thus given by

$$\sigma_{1,2} = -\tfrac{1}{2}[b^2(a_1 + a_2) + c_2(\mathscr{R} - \mathscr{R}_{\mathrm{II}})] \pm \{\tfrac{1}{4}[b^2(a_1 - a_2) + c_2(\mathscr{R} - \mathscr{R}_{\mathrm{II}})]^2 + c_3 b^2(\mathscr{R} - \mathscr{R}_{\mathrm{II}})\}^{\frac{1}{2}}. \tag{4.3}$$

When this expression is evaluated in the limit $b \to 0$,

$$\sigma_1 = b^2\left(\frac{c_3}{c_2} - a_1\right) - b^4 \frac{c_3}{c_2^2(\mathscr{R} - \mathscr{R}_{\mathrm{II}})}\left(a_2 + \frac{c_3}{c_2} - a_1\right) + \ldots, \tag{4.4a}$$

$$\sigma_2 = -b^2\left(\frac{c_3}{c_2} + a_2\right) - c_2(\mathscr{R} - \mathscr{R}_{\mathrm{II}}) + b^4 \frac{c_3}{c_2^2(\mathscr{R} - \mathscr{R}_{\mathrm{II}})}\left(a_2 + \frac{c_3}{c_2} - a_1\right) + \ldots, \tag{4.4b}$$

are obtained. In the present case $a_1 < c_3/c_2$ holds and a positive growth rate is found. σ_1 reaches its maximum $\sigma_{1\mathrm{m}}$ at the value b_{m}^2,

$$\sigma_{1\mathrm{m}} \approx \tfrac{1}{4} b_{\mathrm{m}}^2 \left(\frac{c_3}{c_2} - a_1\right) \quad \text{with} \quad b_{\mathrm{m}}^2 \approx \tfrac{1}{4}(c_3 c_2 - a_1 c_2^2)(\mathscr{R} - \mathscr{R}_{\mathrm{II}}) \left[\frac{c_3 a_2 - c_3^2}{c_2 - a_1 c_3}\right]^{-1}, \tag{4.5}$$

but these expressions provide only a rough estimate since the conditions for the validity of (4.4) are not well satisfied at $b = b_{\mathrm{m}}$. Although the matrix elements in the determinant vary continuously as $\mathscr{R} - \mathscr{R}_{\mathrm{II}}$ changes from negative to positive values, the second derivative $\partial^2\sigma/\partial b^2$ exhibits a discontinuity. In figure 7 (*a*, *b*) numerical computations of the two eigenvalues are displayed for different values of b for both the ordinary and the wavy twist case. In the latter case the growth rates of the

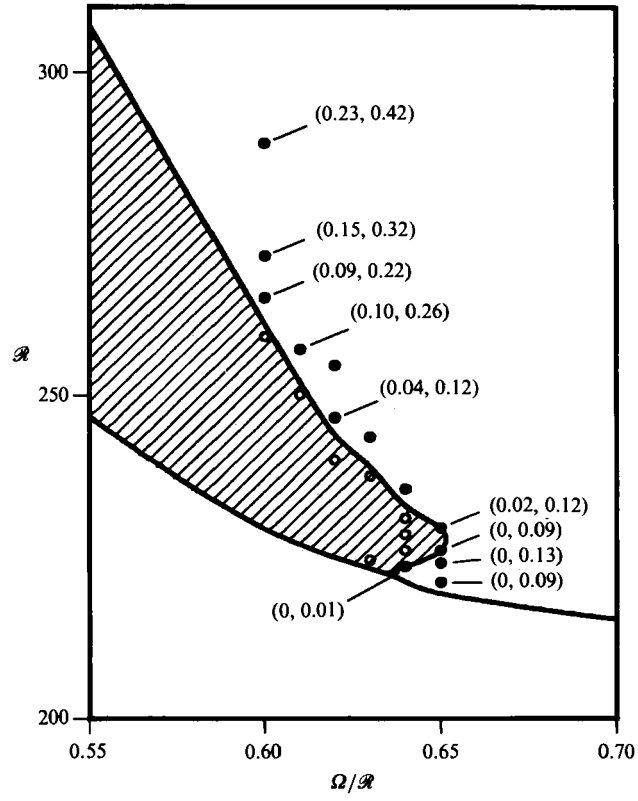

FIGURE 8. Detailed plot of the stable regime of ordinary twists (hatched area) for $\gamma = 2.3$. The solid dots represent an unstable solution. The numbers in the brackets are the Floquet parameters (b, d) for which the growth rate becomes maximal. The circles denote stable twist solutions.

shifting and the wavy twist instability approach each other closely at the critical Reynolds number $\mathscr{R}_{II}$ for finite values of b. The disturbance eigenvectors thus change significantly at $\mathscr{R} = \mathscr{R}_{II}$. The values a_1, a_2, c_1, c_2, c_3 corresponding to the cases displayed in figure 7 (a, b) are given approximately by

$$a_1 = 2.79, \quad a_2 = 8.08, \quad c_1 = 0.199, \quad c_2 = 0.398, \quad c_3 = 3.63, \tag{4.6a}$$

$$a_1 = 2.37, \quad a_2 = 3.07, \quad c_1 = 0.182, \quad c_2 = 0.363, \quad c_3 = 1.94. \tag{4.6b}$$

Basically the instability of twists is caused by a relatively small value of c_2, which indicates that the non-axisymmetric components of the twist solutions do not grow strongly as the critical Reynolds number is exceeded. The non-diagonal terms in the matrix (4.2) thus exert their destabilizing role when c_3/c_2 becomes sufficiently large.

The coupling between twist and shifting modes occurs throughout the parameter regime, but it does not lead to unstable situations in every case. Ordinary twists and wavy twists both exhibit regimes of stable solutions. As figure 6 shows, these regimes are located at low rotation rates for ordinary twists and at high rotations rate for wavy twists. The stable regime of ordinary twists is bounded towards high Reynolds numbers by a skewed varicose instability. This instability tends to change the wavelength and appears first at arbitrary small Floquet parameters. Beyond the stability boundary the largest growth rates are achieved for non-vanishing values of b and d, however. Figure 8 shows the bounds of the regime in more detail for the case $\gamma = 2.3$. The angle $\theta = \arctan(b/d)$ between the wave vector of the instability and

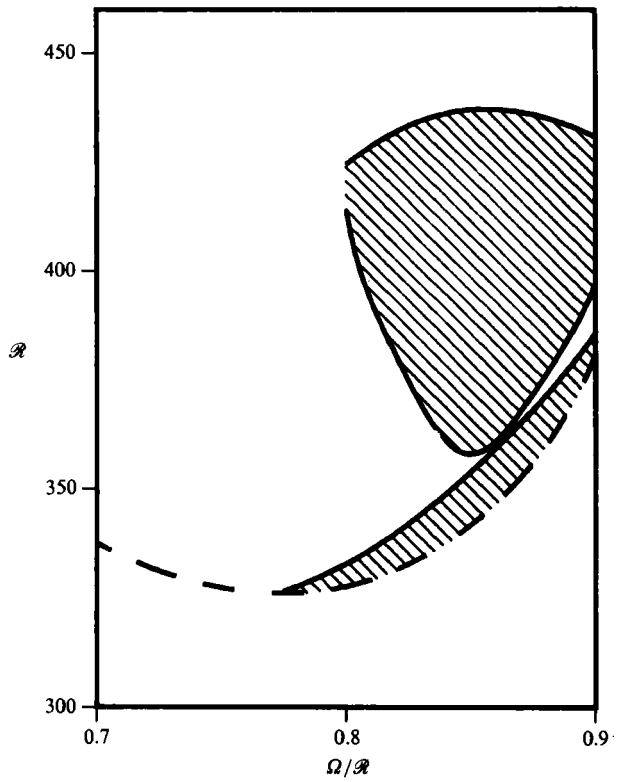

FIGURE 9. Detailed plot of the stable regime of wavy twists (hatched area) for $\gamma = 3.1$. Two separated stable regimes exist. The lower regime becomes unstable towards higher Reynolds numbers for Floquet parameters $b \neq 0$ while the upper regime is bounded toward higher Reynolds numbers by an instability with $d \neq 0$.

the azimuthal axis is approximately 60°. This angle does not change much as γ varies.

The regimes of stable wavy twist solutions are not as simple as those of ordinary twists and differ in character. For sufficiently small γ there are no stable wavy twists. At high γ ($\gamma > 2.7$) there are two separate stability regions, one at low and the other at high Reynolds numbers. When γ is decreased to values of about $\gamma = 2.7$ the two regions first meet at one point and then form a single regime. Also, the regime of stable solutions becomes smaller with decreasing γ until it disappears. Again, the solutions are destabilized by a wavelength-changing instability. But in contrast to the case of ordinary twist solutions, the wave vectors of the most unstable modes are not skewed. In general the instability affects the axial wavelength ($b \neq 0, d = 0$) except for the upper part of the regime, where the instability first sets in for $d \neq 0$ and $b = 0$. Figure 9 presents a detailed picture for the case $\gamma = 3.1$.

In §3.2 we have seen that convergence properties of the finite-amplitude solutions were satisfactory. Here we want to consider the convergence properties of the stability analysis. We have chosen the case of wavy twists because the strongest growing instabilities occur for $d = 0$ or for $b = 0$ in this case. It is thus relatively easy to increase the truncation parameters. We compare the growth rate for solutions obtained with $N_T = 10$ and $m_T = 4$ at several Reynolds numbers along a line of constant γ and constant $\Omega/\mathscr{R}$ with those obtained for $N_T = 11$ and $m_T = 5$. The results are shown in figure 10 for $\gamma = 2.7$ and $\Omega/\mathscr{R} = 0.80$. We conclude that the

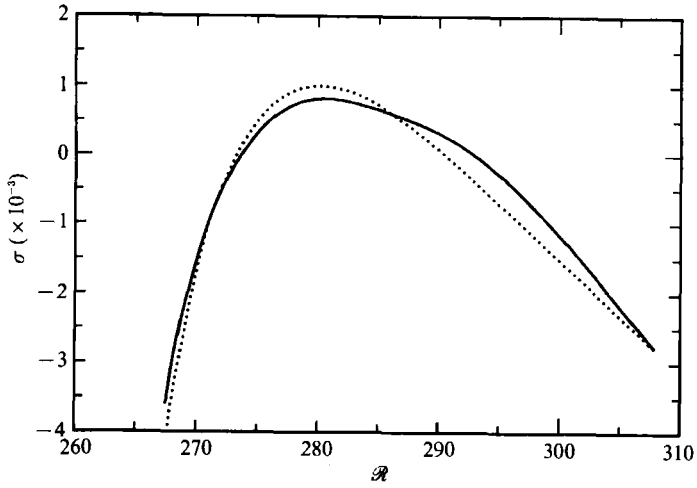

FIGURE 10. Convergence of the largest eigenvalue σ for the case of wavy twists ($\gamma = 2.7$ and $\Omega/\mathscr{R} = 0.8$). Solid curve, $N_T = 10$ and $m_T = 4$; dashed curve, $N_T = 11$ and $m_T = 5$.

eigenvalues calculated with our standard choice of truncation parameters are reliable. All features such as, for example, the island of unstable solutions, are well represented.

5. Conclusions

Twisted vortices are an important tertiary flow phenomenon in the Taylor–Couette system with corotating cylinders. They develop from axisymmetric Taylor–Couette vortices via a forward bifurcation. The correspondence between the theoretical predictions for the onset of twists and experimental data on twist vortices given by Andereck *et al.* (1983) is satisfactory. The photographs of twist flows show the 'in-phase' symmetry of ordinary twists at low rotation rates. The stability regimes of ordinary twists and wavy twists are sufficiently large to explain the experimental findings of stable twist structures.

We have also shown that for a considerable range of the parameters twists are unstable with respect to a wavelength-changing instability. The mechanism of this instability is unusual. Usually the growing mode saturates, when the new structure has been established. But here an axial wavelength-changing instability is caused by a coupling between the twist and the shifting modes. This instability occurs at intermediate rotation rates $\Omega/\mathscr{R}$ for both symmetry classes. The ultimate fate of these unstable twists is not clear. When the instability causes an increase of the axial wavelength then the Reynolds number becomes subcritical and the vortices will become axisymmetric again. When the axial wavelength is decreased no stable stationary solution can be reached. Another possibility is a modulation leading to a non-uniform wavelength. Patterns with 'domains' of large and small vortex pairs have indeed been observed in experiments (Andereck & Baxter 1988). The authors mention a sideband instability for this regime and comment that 'the system seems unable to choose a new wavelength'. This description of the instability fits well with our findings. The domain states are observed experimentally at rotation rates $\Omega/\mathscr{R}$ of about 0.25 and at Reynolds numbers of about 1400, however, which is beyond the regime where our analysis has been carried out. On the other hand, the unstable

regime that we found in our calculations represents only a small strip in the diagrams by Andereck *et al.* (1983). It seems likely that the same mechanism is working in both cases.

The calculations have been carried out on the Cray XMP of the HLRZ of the KFA Jülich and in part on the Cray XMP of the Leibniz-Rechenzentrum München.

REFERENCES

ANDERECK, C. D. & BAXTER, G. W. 1988 An overview of the flow regimes in a circular Couette system. In *Propagation in Systems Far From Equilibrium, Proc. Workshop, Les Houches, France, March 10–18, 1987*, pp. 315–324. Springer.

ANDERECK, C. D., DICKMAN, R. & SWINNEY, H. L. 1983 New flows in a circular Couette system with co-rotating cylinders. *Phys. Fluids* **26**, 1395–1401.

ANDERECK, C. D., LIU, S. S. & SWINNEY, H. L. 1986 Flow regimes in a circular Couette system with independently rotating cylinders. *J. Fluid Mech.* **164**, 155–183.

BAXTER, G. W. & ANDERECK, C. D. 1986 Formation of dynamical domains in a circular Couette system. *Phys. Rev. Lett.* **57**, 3046–3049.

CHANDRASEKHAR, S. 1961 *Hydrodynamic and Hydromagnetic Stability*. Oxford University Press.

IOOSS, G. 1986 Secondary bifurcations of Taylor vortices into wavy inflow or outflow boundaries. *J. Fluid Mech.* **173**, 273–288.

MARCUS, P. S. 1984 Simulation of Taylor–Couette flow. Part 2. Numerical results for wavy vortex flow with one travelling wave. *J. Fluid Mech.* **146**, 65–113.

MOSER, R. D., MOIN, P. & LEONHARD, A. 1983 A spectral numerical method for the Navier–Stokes equation with applications to Taylor–Couette flow. *J. Comput. Phys.* **52**, 524–544.

NAGATA, M. 1986 Bifurcations in Couette flow between almost corotating cylinders. *J. Fluid Mech.* **169**, 229–250.

NAGATA, M. 1988 On wavy instabilities of the Taylor–vortex flow between corotating cylinders. *J. Fluid Mech.* **188**, 585–598.

NAGATA, M. & BUSSE, F. H. 1983 Three-dimensional tertiary motions in a plane shear layer. *J. Fluid Mech.* **135**, 1–26.

WEISSHAAR, E., BUSSE, F. H. & NAGATA, M. 1990 Instabilities of tertiary flow in the Taylor–Couette system. In *Topological Fluid Dynamics, Proc. IUTAM Symp., Cambridge UK 13–18 August 1989* (ed. H. K. Moffatt & A. Tsinober), pp. 709–716. Cambridge University Press.